# Dynamic turning of 13 cm robot comparing tail and differential drive

A.O. Pullin† N.J. Kohut† D. Zarrouk* and R. S. Fearing*

***Abstract*— Rapid and consistent turning of running legged robots on surfaces with moderate friction is challenging due to leg slip and uncertain dynamics. A tail is proposed as a method to effect turns at higher yaw frequencies than can be obtained by differential velocity drive of alternate sides. Here we introduce a 100 mm scale dynamic robot - OctoRoACH - with differential-drive steering and a low-mass tail to investigate issues of yaw rate control. The robot without tail is under-actuated with only 2 drive motors and mass of 35 grams including battery and control electronics. For some surface conditions, OctoRoACH can maintain heading or turning rate using only leg velocity control, and a basic rate-gyro-based heading control system can respond to disturbances, with a closed-loop bandwidth of approximately 1 Hz. Using a modified off-the-shelf servo for the tail drive, the robot responds to turning commands at 4 Hz and up to 400°/sec.**

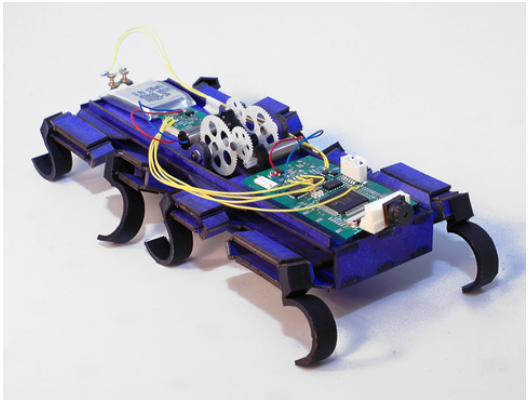

Fig. 1. OctoRoACH robot with independent drive of each side.

## I. Introduction

Small crawling robots are promising for future applications in reaching spaces which are inaccessible for larger robots or are dangerous for people, such as search and rescue, or hazardous exploration. There are a variety of recent small robot developments including small-scale jumping robots [14], [3], and small finger-sized crawling robots such as the milliRoACH (Hoover et al. 2008 [9]) and a piezo-electrically driven robot made from carbon fiber microstructures (Baisch and Wood 2010 [2]).

Small robots have been shown to be capable of running at more than 10 body lengths per second, e.g. Mini-Whegs [17], iSprawl [12], DASH [4], and DynaRoACH [10]. There have been a variety of steering means proposed for dynamic running robots, including differential velocity drive in RHex [19], or actively changing leg kinematics such as in Sprawlita [5] and iSprawl [16]. These steering methods have worked reasonably well on relatively flat surfaces, but may be susceptible to heading disturbances on more complicated terrain.

In this paper, we briefly review previous dynamic turning and then present the design of the OctoRoACH 8-legged crawling robot, including mechanics and instrumentation system. We next describe two steering systems, first a differential leg velocity steering system, and next a novel tail-driven steering method. A closed-loop steering system using a reference turning rate is implemented using a rate gyro. The tail steering system uses changing angular momentum to control yaw rate. The two steering methods are compared using a sinusoidal steering command.

The work was supported by the Army Research Laboratory under the Micro Autonomous Systems and Technology Collaborative Technology Alliance.

Corresponding author: pullin@eecs.berkeley.edu, † Dept. of Mechanical Engineering, University of California, Berkeley

∗ Dept. of Electrical Engineering and Computer Science, University of California, Berkeley

### A. Previous work in Dynamic Turning Control

There have a been variety of methods used for steering small robots. The simplest static methods can include independently controlling stroke length of legs on each side, as the MEDIC robot Kohut et al. 2011 [13] which employs 4 actuators. A practical approach in Mini-Whegs [17] for high speed steering uses a servo to drive an articulated steering linkage. The 2.4 gram milliRoACH [9] uses a quasi-static tripod drive, where asymmetrical drive of the tripods generates a turning moment. A recent piezo-electrically driven hexapod with 6 actuators (Baisch and Wood [2]) allows individual control of leg drive strength in fore-aft direction, and hence fine control for steering.

The lateral leg stability model has been used by [6], [18] to explain how passive mechanical properties of leg stiffness, leg placement, and leg velocity can stabilize the robot heading in the face of disturbances. This model has been used by several researchers to design steering systems for dynamic robots, notably in the Sprawlita [5] and iSprawl [12] hexapod robots. For example, in iSprawl, a main drive actuator with push-pull cable is used for all legs in parallel, while small servos can be used to actively change the position of a leg during a stroke. The kinematic space for effective turning of i-Sprawl was examined by [16]. Recently, Hoover et al. 2010 [10] proposed modulation of leg impedance to cause turning, and achieved a turning rate of 100 degrees per second. (However, in [10] leg impedance was changed by swapping legs, rather than by using actuator control.)

The original RHex (Saranli et al. [19]) controlled turning

rate by setting differential leg rotation velocity on each side of the robot. Similarly, Tsujita et al [21] calculated the leg velocity on each side of a quadruped for a given body velocity and turning radius. In this paper OctoRoACH uses the same strategy, but with control of turning using gyro feedback. There has been little published work on closed-loop heading control for small dynamic legged robots. Lee et al. [15] examine closed-loop steering with the addition of a mechanical antenna sensor.

Another method of turning is to use the dynamics of a tail to induce transient moments. There has been work on tails for turning in free-fall, such as the work of Jusufi et al. [11] on righting in lizards. Takita et al. [20] considers generating yaw moments in the bipedal TITRUS robot using neck and tail accelerations during pivot turns. Here, we show that OctoRoACH can be turned using a tail to affect a change in angular momentum. (For a fish robot, Hirata et al. [7] does mention this turning mode as a way to turn while the robot is stationary in water.)

## II. Robot Design

The previous generation of minimally actuated 6-legged robots (DynaRoACH, Hoover et al. 2010 [10]) used a single drive motor and an alternating tripod gait, where steering moments were provided by changing the stiffness of a single leg. Here, OctoRoACH uses an independent drive train for each side of the robot; similar to the system on some tracked vehicles. In the current design, the left and right leg strides are not synchronized. An eight-leg configuration was chosen to maximimize pitch stability by avoiding a possible intermittent bipedal gait of the opposing center legs which might occur in a dual-drive hexapod configuration.

For rapid fabrication and ease of design changes, OctoRoACH is fabricated using a stacked, laser-cut lamination prototyping process [8] that is a scaled version of smart composite microstructures (SCM) [22]. The OctoRoACH design is compared to the DynaRoACH design in Table I. The present OctoRoACH robot is significantly over target weight as an extra battery, motor, and transmission were added in addition to those used by DynaRoach. However, the chassis weight can be reduced by aggressive use of reinforcing, and use of materials such as carbon fiber composites instead of the present paper board. The robot is driven by 2 DC brush motors through two independent 2 stage gear transmissions.

### A. Kinematic Transmission Design

The OctoRoACH design follows that of DynaRoACH described in Hoover et al. 2010 [10] (see [10] for more detail on the kinematic design). As in DynaRoACH, the leg drive kinematics are comprised of two primitive single degree-of-freedom mechanisms: the slider-crank linkage and the parallel fourbar. Here the mechanism has been duplicated for independent drive of the legs on each side. Rear and side views of the ideal kinematics of the robot are shown in Fig. 2. The slider crank linkages enable ab- and adduction of the legs, while fourbar linkages enable protraction and retraction.

| | DynaRoACH | OctoRoACH |
|---|---|---|
| Total Mass | 23.7 gm | 35 gm |
| Body Size | 100x45x30 mm | 130x60x30 mm |
| Maximum speed | 1.4 m/s | 0.5 m/s |
| Maximum stride freq. | 20Hz | 25 Hz |
| Motor | Didel MK07-3.3 | Vamp |
| Battery | 90mA-Hr LiPO | 300 mA-hr |
| Microcontroller | dsPIC33F | dsPIC33F |
| Communications | Bluetooth | Zigbee |

TABLE I
Robot physical parameters for DynaRoACH [10] and OctoRoACH

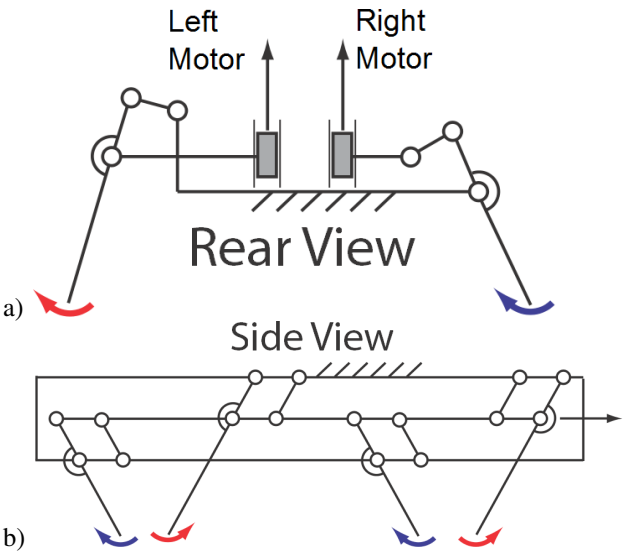


Fig. 2. Ideal robot kinematics demonstrating the kinematic coupling enabling fore-aft and in-out motion of legs. The two sides of the robot are driven independently. The motor outputs are aligned with the sagittal plane and a crank provides the vertical and fore-aft motion depicted in each figure. a) Rear view of the ideal robot kinematics: ab- and adduction of leg pairs on each side occurs out of phase when the middle member of the linkage is translated vertically. b) Side view of the ideal robot kinematics: protraction and retraction of the legs is controlled by motion of the middle member in the fore-aft direction. The alternate pairs move approximately 180° out of phase with each other.

### B. Leg Design

We use similar legs (shown in Fig. 1) as described in [10]:

> *We have chosen a semi-circle C shape for the robot's leg similar to the design used on the RHex robot [19]. The leg is manufactured by molding using a stiff polyurethane elastomer with 20% softener by weight (PMC-790 rubber and SO-FLEX softener, Smooth-On, Inc.). The C shape offers three primary advantages: lower vertical stiffness, lateral collapsibility for obstacle climbing, and a rolling instead of point ground contact.*

The legs are soft enough to obtain a relatively high friction coefficient on smooth hard surfaces ($\mu_s \approx 0.7$). Also, due to the anisotropic C-shape, the feet engage very well on rough, soft surfaces such as carpet ($\mu_s \approx 2.0$).

### C. Power, Communication, and Control Hardware

The robot uses the dsPIC33FJ128MC706-based microcontroller board described in [13] for control. As shown in Fig. 3, the board contains an Atmel AT86RF231 Zigbee transceiver, ADXL345 3 axis accelerometer, and an Invensense 3 axis ITG-3200 gyro. A single NMOSFET drive per motor is driven using pulse width modulation (PWM) providing forward direction only. Two analog-to-digital converter channels on the PIC are used to sample the NMOSFET drain voltage during the off portion of the pulse width modulation signal, $V_{s1}$ and $V_{s2}$. Assuming the battery voltage $V_{BAT}$ is approximately constant with the motor off, the motor back EMF $V_{EMF} \approx V_{BAT} - V_s$.

Data including roll, pitch, yaw rates, accelerations, and motor back EMF is recorded during experiments into a 4MB Flash memory, and downloaded through the wireless link after runs to a host processor for off-line data processing. With cell-phone camera, the processor board has mass $\approx$ 1.5 gram.

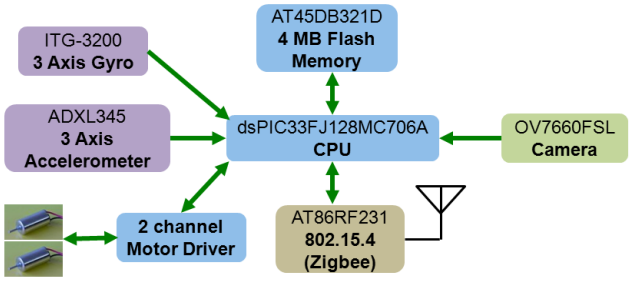


Fig. 3. Block diagram of ImageProc2.2 controller board.

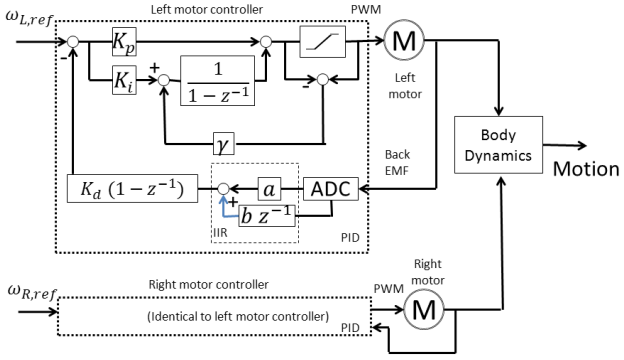


Fig. 4. Block diagram of velocity control loops using motor back EMF.

## III. Dynamic Turning Control in OctoRoACH

We first consider dynamic turning control using differential leg velocity, and then tail-induced turning.

### A. Open loop velocity control

As mentioned, OctoRoACH uses differential velocity control to steer. The control system consists of a velocity control loop for each motor using back EMF data as a proxy for velocity. The standard digital proportional+integral+derivative controller, as shown in Fig. 4, runs at 1 kHz. Due to the motor slider-crank angle and joint stiffness as well as leg contact loads, the motor sees a phase dependent load which makes smooth velocity control difficult. Also, since the motor PWM is unidirectional, the controller can not slow down the motor to compensate for the release of stored elastic energy. Thus the velocity control should be considered more as setting a target cyclic rate rather than tracking a constant velocity with a leg stride.

Fig. 5 shows the principle of differential steering in the case without leg slip, for example when the commanded leg velocity is such that the leg thrust is within the static friction regime. This model requires slip at all feet while turning, and with a pair of feet in contact on each side, the leg stride is not tangential to the desired turning arc, where $r$ is the vector to the turn center. (Typically, an articulated body such as in [1], [17] allows front and rear sections to be tangent to the arc, reducing foot slip requirements. For simplicity in the drive system, OctoRoACH is not articulated.)

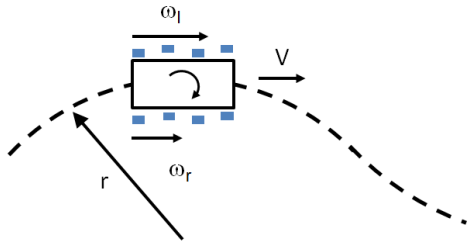


Fig. 5. Standard concept of differential steering, with faster leg angular rate on outside of turn.

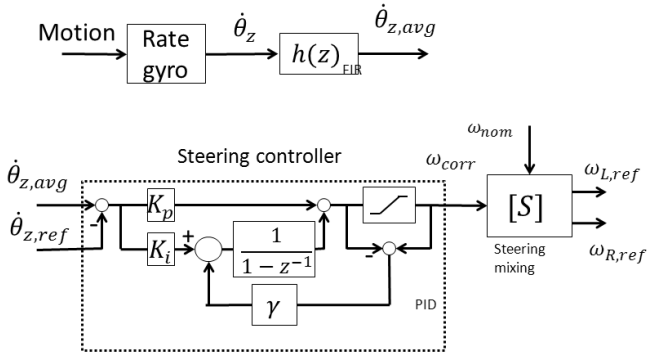


Fig. 6. Block diagram of turning rate control using rate gyro feedback.

### B. Gyro based closed loop control

The nominal rate of turning of the robot is proportional to the difference between the right and left leg stride rates; that is, $\omega_{nom} \sim \omega_R - \omega_L$. The actual turning rate of the robot is measured by a digital IIR low-pass-filter-smoothed rate gyro signal $\dot{\theta}_{z,avg}$ and is controlled to a reference turning rate $\dot{\theta}_{z,ref}$ using a standard digital PID control loop. Fig. 6 shows the turning rate control system using PID control. The updates to commanded leg cyclic rate occur at 300 Hz.

### C. Tail Based Turning

As illustrated in Fig. 7, a simple model to predict the behavior of the tail steering has been developed to provide insight into the robot's dynamic behavior. This is a 2-D, two body model, with the robot represented as a body with mass $m_b$ and yaw inertia $I_b$. The tail is represented as a point mass $m_t$, located on a massless rod of length $l$ away from the rear of the body. We can express the angular momentum of the two-body system as a function of the above parameters, the body angle $\theta$, and the tail angle (relative to the body), $\phi$. Taking the time derivative of the angular momentum allows us to predict how the body angle will change for a given change in tail angle. It is assumed that there is a friction torque resisting body rotation that is a function of body size, mass, and friction coefficient. Effects of translation have been neglected.

Using differential equation solvers in MATLAB, we can simulate the tail performance at a wide range of parameters. The angular momentum $H$, neglecting effects of translation, is given by:

$$H = \left(m_t \frac{b^2}{4} + m_t l^2 + m_t bl\cos(\phi) + I_b\right)\dot{\theta} + \left(m_t l^2 + m_t \frac{bl\cos(\phi)}{2}\right)\dot{\phi} \quad (1)$$

The rate of change of angular momentum is given by:

$$\dot{H} = -blm_t \sin(\phi)\dot{\theta}\dot{\phi} - \frac{1}{2}blm_t \sin(\phi)\dot{\phi}^2 + \left(I_b + \frac{b^2 m_t}{4} + l^2 m_t + blb_t\cos(\phi)\right)\ddot{\theta} + \frac{1}{2}lm_t\left(2l + b\cos(\phi)\right)\ddot{\phi} \quad (2)$$

### D. Experimental methods

Batteries (300 mA-hr LiPO, Full River) were charged as needed. A low pile carpet was used as a substrate for differential steering, with vinyl floor tile used as the substrate for tail steering tests. Transient closed-loop response tests were conducted on across foam-core poster board and soft play mat surfaces. During a run, back EMF and gyro data were stored to Flash memory at a rate of 150 Hz, and were downloaded over a wireless connection at the end of a run.

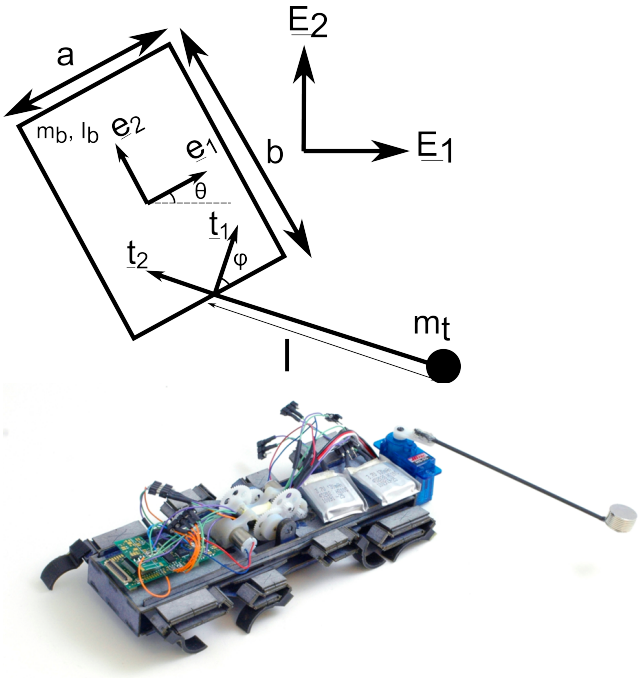


Fig. 7. Model of geometry for tail steering, and modified OctoRoACH with servo motor driven tail.

## IV. Results

### A. Differential Drive Open Loop Performance

The differential steering method assumes that the legs do not slip significantly at high leg velocities. Coefficient of friction was measured on vinyl tile for various leg frequencies using an inclined plane. This was done by running the robot at different leg frequencies, and changing the slope until the robot neither ascended nor descended. The tangent of the slope angle is the effective coefficient of friction during the experiment. The results of this experiment can be seen in Fig. 8.

As shown, the maximum coefficient of friction is at low leg frequencies. Above 7 Hz on tile, the legs slip significantly. This has important implications for how the robot turns. The yaw rate of the robot is a function of its forward velocity on its left and right sides.

$$\omega_{nom} = \dot{\theta}_z = \frac{\dot{x_r} - \dot{x_l}}{r} \quad (3)$$

If the controller is unable to increase the velocity on one side due to slipping, the robot may not turn. For these low friction situations, using the tail may be more advantageous.

It is likely that for higher friction surfaces such as carpet, coefficient of friction would remain high at higher leg frequencies, and this problem would be less likely.

The robot open-loop turning rate behavior was characterized on a high friction, low slip carpet, which had static coefficient of friction (c.o.f.) $\mu_s \approx 2.0$ and sliding c.of. $\mu_k \approx 1.4$. The high friction is likely due to the curved

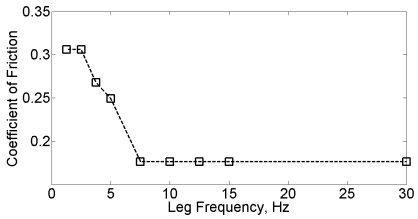


Fig. 8. Estimated coefficient of friction on vinyl tile surface using friction angle measurement. Beyond 7 Hz, legs are slipping on surface, limiting thrust.

robot feet digging into ridges on the carpet. The maximum stride rate for the unloaded robot is approximately 25 Hz, corresponding to a crank frequency of 12.5 Hz. Using the back-EMF based velocity controller, a set of commanded leg cyclic rate differences $\omega_R - \omega_L$ was applied and the steady state turning rate was estimated from the smoothed gyro data $\dot{\theta}_{z,avg}$. (The smoothing of gyro data removes most of the intra-stride angular rate changes.)

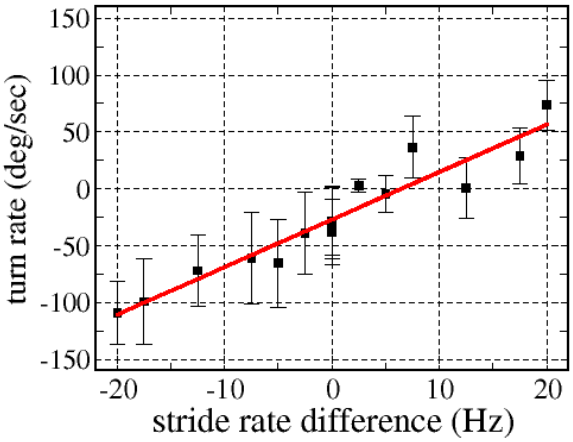


Fig. 9. Result of open loop steering using velocity control on left and right side motors on carpet. Due to imbalance from construction variation, battery charge differences, and robot dynamics, open-loop steering, while approximately linear, has large offsets in turning rate.

Figure 9 shows the resulting turn rate for a range of stride rate differences between right and left sides. The turning rate is proportional to stride rate, with turn rate constant of $4.2°s^{-1}\text{Hz}^{-1}$. The error bars show $\pm 1 s.d.$ over a single run. The large offset of $-27°s^{-1}$ for nominal equal commanded left and right leg stride frequencies shows the need for closed loop control of turning rate. This offset can be due to construction variation such as higher joint stiffness, kinematic misalignments, or a difference in battery voltage. The robot feet slip very little on the carpet material used, leading to an approximately linear relation between velocity difference and turning rate.

### B. Differental Drive Sinusoidal Response

Fig. 10 shows the gain response of the rate-gyro steering controller on the tailless robot. The input to the steering controller is set such that the commanded yaw rate was a pure sinusoid with a fixed amplitude, i.e. $\dot{\theta}_{z,ref} = A_o \sin(2\pi f t)$.

Because it is expected that steering through differential drive is a traction limited ability, these tests were run on a carpeted surface to provide high traction, and expose the response dynamics of the steering controller. The steering mixing method used was to increase the thrust to the legs on the outside of the turn.

This result demonstrates that the response of the steering controller tracks the commanded input yaw rate closely at low frequencies; the amplitudes chosen for these tests were known to be achievable when turning while running.

At low amplitudes, the yaw variations in the robot during a normal stride are greater than $15°$, as seen in Fig. 9, thus it is difficult to identify the steering controller response. For larger amplitudes of the sinusoidal input, the response is clearer, and we can see a decrease in ability to track the input with increasing frequency.

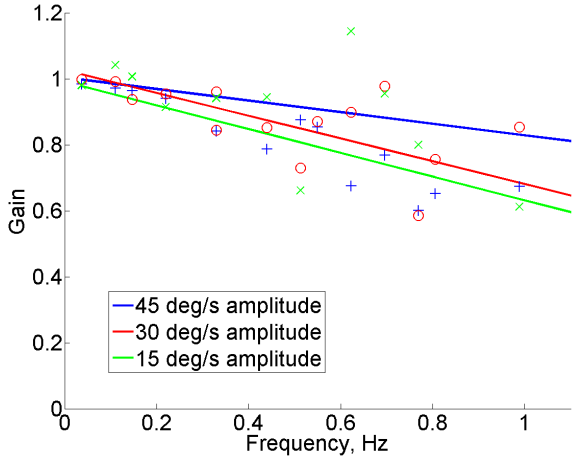


Fig. 10. Steering controller yaw rate magnitude response, where gain is defined as the ratio of the body yaw rate to a sinusoidal commanded input yaw rate, and for several amplitudes. Tests were on a carpet surface, to give very high foot traction. Frequency response is limited by leg slip as well as unmodelled dynamic effects on carpet.

### C. Closed-Loop Steering Transient Response

The differential steering shown in Fig. 9 shows considerable noise. The closed-loop steering system using gyro rate feedback needs to compensate for these disturbances. We can demonstrate the utility of the gyro control by comparing steering responses for open-loop and closed-loop as the robot transitions between different materials.

In the experiment, the two surfaces, poster board and a play mat, had approximately the same height, but the horizontal gap between the surfaces could catch a foot, leading to heading disturbances. There was much run-to-run variation as feet would randomly catch on gaps between surfaces depending on instantaneous leg phase. An overhead camera was used to record runs and correlate events in observed behavior and angular rate data. A representative

open-loop and closed-loop run were selected which illustrate some of the key behaviors observed.

For open loop, the robot was tested with a commanded turning rate of $45°s^{-1}$ making a transition from a surface with $\mu_s = 0.79, \mu_k = 0.65$ to one with $\mu_s = 0.57, \mu_k = 0.47$. Figure 11 shows steady state heading error when the robot transitions from the medium to the lower friction surface. The robot heading, as determined from the integral of $\dot{\theta}_z$, shows nominal open loop turn rate of $45°s^{-1}$ until the transition to the lower c.o.f. material at 1.7 sec, when the feet slip, and the robot only turns at an effective rate of $\approx 25°s^{-1}$.

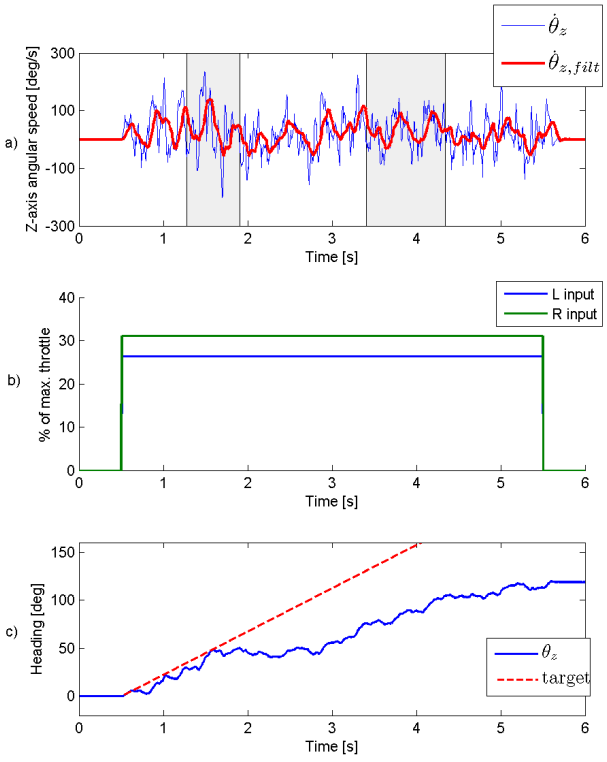


Fig. 11. Result of open-loop steering with desired turn rate of $45°sec^{-1}$. a) Raw and filtered sensed turning rate from gyro. b) Commanded left and right leg stride rates. c) Net heading from integral of rate data. Events are indicated in a) as follows, as extracted from overhead video. t= 0.5 sec: starting on higher friction material. t=1.2 sec: transition from high to low friction material. 1.9 sec $< t <$ 3.3 sec: running on low friction material. 3.3 sec $< t <$ 4.3 sec: crossing transition on low friction material. 4.3 sec $< t <$ 5.7 sec: running on low friction material.

Figure 12 shows results of closed-loop control running on two surfaces. (Again, as in the open-loop case with commanded turning rate of $45°s^{-1}$ and making a transition from a surface with $\mu_s = 0.79, \mu_k = 0.65$ to one with $\mu_s = 0.57, \mu_k = 0.47$.) The gaps in the video sequence correspond to transient events where the robot's foot got caught in the transition between surfaces. Here the left side is commanded to a nominal stride rate of 12 Hz, and the right side is controlled as necessary to maintain a turning rate of $45°s^{-1}$. (Recall that the motor control is unidirectional).

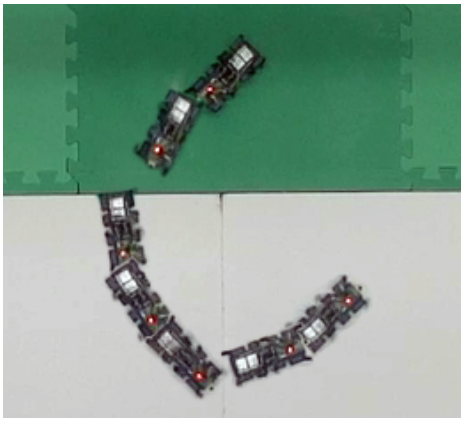

Fig. 12. Selected frames from closed loop steering experiment shown in Fig. 13 (frames at 0.66 second spacing). Discontinuities are due to transient response at transitions between surfaces.

The resulting closed loop response in Fig. 13 clearly shows the transient events at approximately 1.2 sec for the transition from the surface with $\mu_s = 0.79$ to one with $\mu_s = 0.57$, with the middle foot catching in the gap. The robot recovers to its original heading after an approximately 0.4 s transient, and then maintains a turn rate of approximately $45°s^{-1}$ until the gap between foam core boards catches a foot, causing another transient at approximately 2.8 s. Again, after an approximate 0.4 s transient, the robot heading recovers approximately to the original value. Thus the rate gyro PID closed-loop system appears to respond appropriately to both transients and changes in surface friction.

### *D. Tail Drive Sinusoidal Response*

Figure 14 shows the ratio of body yaw rate to tail yaw rate for various frequencies and tail amplitudes. That is, the tail commanded angle $\phi(t) = \phi_o \sin(2\pi ft)$, where amplitude tests at $\phi_o = 20°, 30°, 40°$ are used, and this is compared to the yaw rate of the body. In an absolute sense, we measured a maximum body yaw rate of $400°$ per second with 4 Hz tail drive.

Figure 15 shows that the model results line up well with the experimental data at low frequencies. The model diverges at high frequencies due to the fact that the slew rate limit of the servo is not modeled. The friction used in the model comes directly from the experiment shown in fig. 8.

## V. Discussion and Conclusions

As shown in Table II OctoRoACH has very small turning radius for its size due to differential leg velocity steering, albeit at zero forward velocity. With H-Bridge motor drivers to allow bidirectional motion of each side, zero radius turns are possible with the OctoRoACH robot. Previous SCM crawling robots such as DASH [4], miniRoACH [9], and DynaRoACH [10], due to being underactuated, could only turn

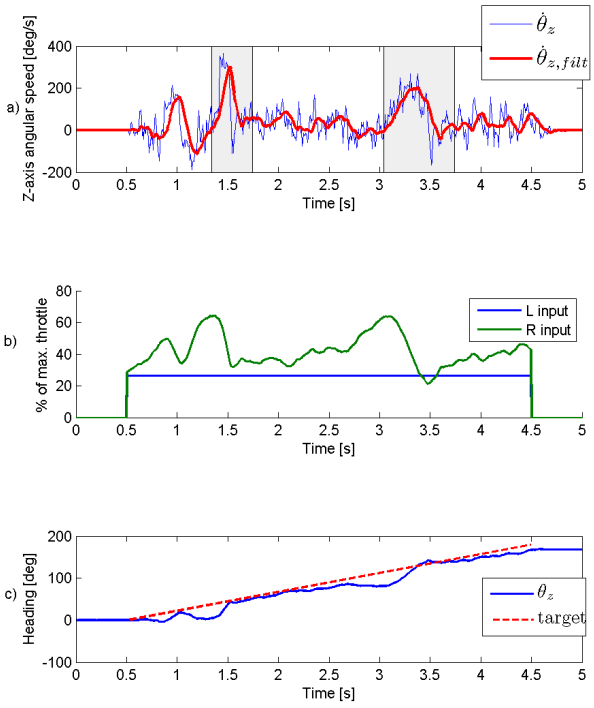


Fig. 13. Result of closed-loop steering with desired turn rate of $45°sec^{-1}$. Transients resulting from foot catching at boundaries between surfaces are marked, and show recovery to original heading.

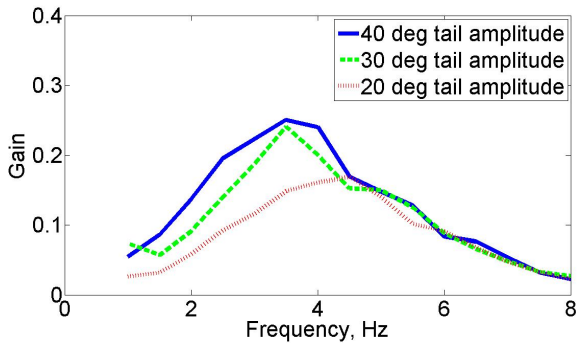


Fig. 14. Body yaw rate gain as a function of tail excitation frequency for three tail amplitudes (peak amplitude). Gain is defined as the ratio of body yaw rate to tail yaw rate. Frequency response is limited by tail servo slew rate limit of 360 degrees per second, which corresponds to 90 degrees at 4 Hz.

while moving forward. Similarly, since iSprawl and Mini-Whegs turn by modifying kinematics during running, low forward speed turning rates will be reduced. The tank-style turning used by RHex and here by OctoRoACH provides a good compromise between performance and actuation complexity.

The tail steering presented here allows very quick turning (up to 400 degrees per second), although this cannot turn the robot further than 90° due to servo angle limits. A custom actuator with a higher bandwidth would allow even higher performance of the tail, as indicated by the results of the model. These two steering modes could be used depending

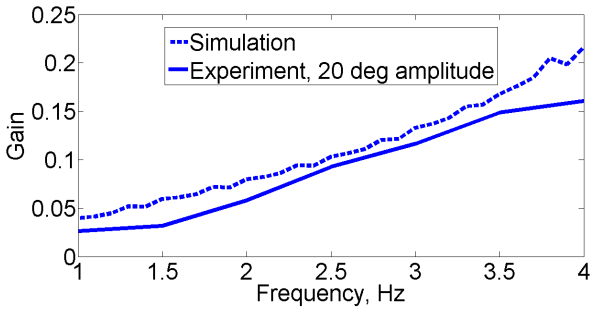


Fig. 15. Experimental and simulated body yaw rate gain as function of tail excitation frequency. Done at position amplitude $\phi(t)$ of 20 degrees. Servo response rolls off at 4 Hz, so the model is not valid above that frequency.

on the situation. If sustained turning is necessary or if the robot is on a high friction surface, differential steering is very effective. If very quick turning is required, as in an evasive maneuver, or if on a low friction surface, tail steering can be effectively applied.

OctoRoACH is still early in its design cycle and has not yet had the mechanical tuning of leg and body compliance (the robot suspension system) which has allowed DASH and DynaRoACH to run stably at better than $1ms^{-1}$. A similar structural tuning for OctoRoACH could improve open-loop yaw stability during running. However, even with a more optimal structural tuning, there are variations in robot construction parameters and even more importantly, surface properties, which can limit the range of acceptable parameters for passive yaw stabilization. Hence, active control of yaw rate using a rate gyro, such as used here for OctoRoACH, has the potential for significantly improving heading stabilization.

Future work will be needed to test the robustness of heading control on more challenging surfaces, such as terrain with roughness greater than leg length. A custom high performance actuator would provide a major improvement for the tail. In addition, the tail could be used as a multi-functional feature, to regulate balance on rough terrain as well as providing steering.

TABLE II

A COMPARISON OF SOME SMALL DYNAMIC LEGGED ROBOTS.

| Robot | Size cm | Mass (gm) | Turn Radius (cm) | Climb (cm) |
|---|---|---|---|---|
| miniRoACH [9] | 3 | 2.4 | 2.5 | 0.1 |
| DASH [4] | 10 | 16 | 20 | 5.5 |
| dynaRoACH [10] | 10 | 24 | 30 | $> 1$ |
| octoRoACH | 13 | 35 | 2.7 ($0ms^{-1}$) 33 ($0.5ms^{-1}$) | $> 1$ |
| octoRoACH + tail | 23 | 52 | 0 ($0ms^{-1}$) 57 ($0.1ms^{-1}$) | $> 1$ |
| Mini-Whegs [17] | 9 | 146 | 17.8 | 5.4 |
| MEDIC [13] | 5 | 5.5 | 2.7 | 0.4 |
| i-SPrawl [12] | 16 | 300 | 23 ($1ms^{-1}$) | $> 2$ |
| RHex [19] | 53 | 7000 | 200 | $> 20$ |

## VI. Acknowledgements

We thank Aaron Hoover for use of the DynaRoACH design, Stan Baek for the ImageProc CPU board, Jaakko Karras and Kevin Peterson for comments on the manuscript, Paul Samuel for transmissions, and Xiao-Yu Fu for construction and process engineering.

## References

[1] S. Aoi, H. Sasaki, and K. Tsuchiya, "A multilegged modular robot that meanders: Investigation of turning maneuvers using its inherent dynamic characteristics," *SIAM Journal on Applied Dynamical Systems*, vol. 6, no. 2, pp. 348–377, 2007.

[2] A. T. Baisch and R. J. Wood, "Biologically inspired locomotion of an insect scale hexapod robot," in *IEEE/RSJ Int. Conf. on Intelligent Robots and Systems*, Taipei, Taiwan, Oct. 2010.

[3] S. Bergbreiter, "Design of an autonomous jumping robot," in *IEEE Int. Conf. on Robotics and Automation*, Rome, Italy, April 2007.

[4] P. Birkmeyer, K. Peterson, and R. S. Fearing, "Dash: A dynamic 16g hexapedal robot," in *IEEE Int. Conf. on Intelligent Robots and Systems*, St. Louis, MO, 2009.

[5] J. G. Cham, S. A. Bailey, J. E. Clark, R. J. Full, and M. R. Cutkosky, "Fast and robust: Hexapedal robots via shape deposition manufacturing," *The International Journal of Robotics Research*, vol. 21, no. 10-11, pp. 869–882, 2002.

[6] R. J. Full, T. Kubow, J. Schmitt, P. Holmes, and D. Koditschek, "Quantifying dynamic stability and maneuverability in legged locomotion," *Integr. Comp. Biol.*, vol. 42, no. 1, pp. 149–157, 2002.

[7] K. Hirata, T. Takimoto, and K. Tamura, "Study on turning performance of a fish robot," in *First International Symposium on Aqua Bio-Mecanisms*, August 2000.

[8] A. M. Hoover and R. S. Fearing, "Fast scale prototyping for folded millirobots," in *IEEE Int. Conf. on Robotics and Automation*, Pasadena, CA, 2008.

[9] A. M. Hoover, E. Steltz, and R. S. Fearing, "Roach: An autonomous 2.4g crawling hexapod robot," in *IEEE Int. Conf. on Intelligent Robots and Systems*, Nice, France, Sept. 2008.

[10] A. Hoover, S. Burden, X.-Y. Fu, S. Sastry, and R. Fearing, "Bio-inspired design and dynamic maneuverability of a minimally actuated six-legged robot," in *IEEE International Conference on Biomedical Robotics and Biomechatronics. BioRob 2010.*, Sep. 2010.

[11] A. Jusufi, D. T. Kawano, T. Libby, and R. J. Full, "Righting and turning in mid-air using appendage inertia: reptile tails, analytical models and bio-inspired robots," *Bioinspiration & Biomimetics*, vol. 5, no. 4, p. 045001, 2010.

[12] S. Kim, J. E. Clark, and M. R. Cutkosky, "iSprawl: Design and tuning for high-speed autonomous open-loop running," *The International Journal of Robotics Research*, vol. 25, no. 9, pp. 903–912, 2006.

[13] N. Kohut, A. Hoover, K. Ma, S. Baek, and R. Fearing, "Medic: A legged millirobot utilizing novel obstacle traversal," in *IEEE Int. Conf. on Robotics and Automation*, May 2011.

[14] M. Kovač, M. Schlegel, J.-C. Zufferey, and D. Floreano, "Steerable miniature jumping robot," *Autonomous Robots*, vol. 28, no. 3, pp. 295–306, 2010.

[15] J. Lee, S. Sponberg, O. Loh, A. Lamperski, R. Full, and N. J. Cowan, "Templates and anchors for antenna-based wall following in cockroaches and robots," *IEEE Trans. on Robotics*, vol. 24, pp. 130 –143, 2008.

[16] A. McClung, "Techniques for dynamic maneuvering of hexapedal legged robots," Ph.D. dissertation, Stanford University, 2006.

[17] J. M. Morrey, B. Lambrecht, A. D. Horchler, R. E. Ritzmann, and R. D. Quinn, "Highly mobile and robust small quadruped robots," in *Intl Conf on Intelligent Robots and Systems*, vol. 1, 2003, pp. 82–87.

[18] J. Proctor and P. Holmes, "Steering by transient destabilization in piecewise-holonomic models of legged locomotion," *Regular and Chaotic Dynamics*, vol. 13, no. 4, pp. 267–282, 2008.

[19] U. Saranli, M. Buehler, and D. E. Koditschek, "RHex: A simple and highly mobile hexapod robot," *The Int. J. of Robotics Research*, vol. 20, no. 7, pp. 616–631, 2001.

[20] K. Takita, T. Katayama, and S. Hirose, "Development of dinosaur-like robot TITRUS- its dynamics and the motion utilizing the dynamic effect of the neck and tail," in *IEEE/RSJ Int. Conf. on Intelligent Robots and Systems*, Las Vegas, NV, October 2003.

[21] K. Tsujita, H. Toui, and K. Tsuchiya, "Dynamic turning control of a quadruped robot using nonlinear oscillators," in *IEEE/RSJ Int. Conf. on Intelligent Robots and Systems*, Sendai, Japan, October 2004.

[22] R. J. Wood, S. Avadhanula, R. Sahai, E. Steltz, and R. S. Fearing, "Microrobot design using fiber reinforced composites," *J. Mech. Design*, vol. 130, no. 5, May 2008.